PHYSICS

Demonstration of diamond nuclear spin gyroscope

Andrey Jarmola[1,2]*, Sean Lourette[1,2], Victor M. Acosta[3], A. Glen Birdwell[2], Peter Blümler[4], Dmitry Budker[1,4,5], Tony Ivanov[2], Vladimir S. Malinovsky[2]

We demonstrate the operation of a rotation sensor based on the nitrogen-14 (^{14}N) nuclear spins intrinsic to nitrogen-vacancy (NV) color centers in diamond. The sensor uses optical polarization and readout of the nuclei and a radio-frequency double-quantum pulse protocol that monitors ^{14}N nuclear spin precession. This measurement protocol suppresses the sensitivity to temperature variations in the ^{14}N quadrupole splitting, and it does not require microwave pulses resonant with the NV electron spin transitions. The device was tested on a rotation platform and demonstrated a sensitivity of 4.7°/$\sqrt{s}$ (13 mHz/$\sqrt{Hz}$), with a bias stability of 0.4 °/s (1.1 mHz).

INTRODUCTION

Rotation sensors (gyroscopes) are broadly used for navigation, automotive guidance, robotics, platform stabilization, etc. (*1*). Various rotation sensor technologies can be subdivided into commercial and emerging. Commercial sensors include mechanical gyroscopes, Sagnac effect optical gyroscopes, and microelectromechanical systems (MEMS) gyroscopes. Among emerging technologies are nuclear magnetic resonance (NMR) gyroscopes. These sensors use hyperpolarized noble gas nuclei confined in vapor cells (*2*–*8*); they may surpass commercial devices within the next decade in terms of accuracy, robustness, and miniaturization (*9*).

Recently proposed nuclear spin gyroscopes based on nitrogen-vacancy (NV) color centers in diamond (*10*, *11*) are analogs of the vapor-based NMR devices, constituting a scalable and miniaturizable solid-state platform, capable of operation in a broad range of environmental conditions. An attractive feature is that a diamond sensor can be configured as a multisensor, reporting on magnetic field, temperature, and strain while also serving as a frequency reference (*12*–*14*). This multisensing capability is important for operation in challenging environments (*15*).

In this work, we demonstrate a diamond NMR gyroscope using the ^{14}N nuclear spins intrinsic to NV centers. Its operation is enabled by direct optical polarization and readout of the ^{14}N nuclear spins (*16*) and a radio-frequency (RF) double-quantum (DQ) pulse protocol that monitors ^{14}N nuclear spin precession. This measurement technique is immune to temperature-induced variations in the ^{14}N quadrupole splitting (*16*, *17*). In contrast to recent work (*18*, *19*), our technique does not require microwave pulses resonant with the NV electron spin transitions. The advantage of this technique is that it directly provides information about the nuclear spin states without requiring precise knowledge of the electron spin transition frequencies, which are susceptible to environmental influences (*16*, *18*, *20*). The nuclear spin interferometric technique developed in this work may find application in solid-state frequency references (*12*, *21*) and in extending tests of fundamental interactions (*2*, *22*) at micro- and nanoscale (*23*, *24*) to those involving nuclear spins. With further improvements, it may also find use in practical devices such as miniature diamond gyroscopes for navigational applications.

[1]Department of Physics, University of California, Berkeley, CA 94720, USA. [2]U.S. Army Research Laboratory, Adelphi, MD 20783, USA. [3]Center for High Technology Materials and Department of Physics and Astronomy, University of New Mexico, Albuquerque, NM 87106, USA. [4]Johannes Gutenberg-Universität Mainz, 55128 Mainz, Germany. [5]Helmholtz-Institut, GSI Helmholtzzentrum für Schwerionenforschung, 55128 Mainz, Germany.
*Corresponding author. Email: jarmola@berkeley.edu

RESULTS

Experimental setup

Figure 1 shows an experimental setup schematic for demonstration of the diamond gyroscope. The diamond sensor, green diode laser, photodetector, and all optical components are mounted on a 35-cm-diameter rotating platform controlled by a commercial rate table system (Ideal Aerosmith, 1291BL). The diamond is a 400-μm-thick single-crystal plate with an NV concentration of ~4 parts per million (ppm). It is placed in an axial magnetic bias field of 482 G aligned along the NV symmetry axis, providing optimal conditions for optical polarization and readout of ^{14}N nuclear spins (*16*). The bias magnetic field is produced by two temperature-compensated samarium-cobalt (SmCo) ring magnets (<10 ppm/°C). These magnets were designed and arranged in a configuration that minimizes magnetic field gradients across the sensing volume. An aspheric condenser lens is used to illuminate an ~50-μm-diameter spot on the diamond with 80 mW of green (515 or 532 nm) laser light and collect NV fluorescence. The fluorescence is spectrally filtered with band-pass filter (650 to 800 nm) and focused onto one of the channels of a balanced photodetector. A small portion of laser light is picked off from the excitation path and directed to the other photodetector channel for balanced detection. RF pulses for nuclear spin control are delivered using a 160-μm-diameter copper wire placed on the diamond surface next to the optical focus. To reduce the ambient magnetic field noise, we placed a part of the setup including the diamond and magnets inside low-carbon-steel magnetic shields (see section S1).

Rotation detection principle

Rotation was detected by measuring the shift in the precession rate of ^{14}N nuclear spins intrinsic to NV centers in diamond. Figure 2A shows the ground-state energy level diagram of the NV center. The inset shows the ^{14}N nuclear spin states $|m_I\rangle$ within the $|m_S = 0\rangle$ electron spin state manifold. The $|m_I = \pm1\rangle$ states are degenerate at zero magnetic field and separated from $|m_I = 0\rangle$ by ~4.94 MHz because of the nuclear quadrupole interaction. In the presence of an applied magnetic field B, the $|m_I = \pm1\rangle$ states experience a Zeeman shift, and the splitting frequency f_{DQ} between $|m_I = +1\rangle$ and $|m_I = -1\rangle$ is described by the following equation (*16*)

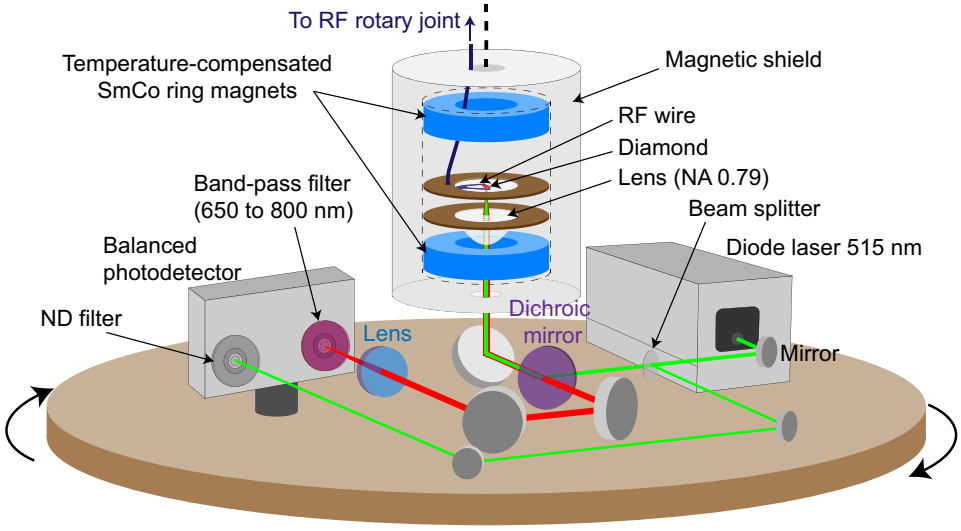

Fig. 1. Experimental setup. Electrical connections for the laser and the photodetector are wired to the rotating platform through slip-ring lines. RF signals are delivered to the platform via a single-channel RF rotary joint. NA, numerical aperture. ND, neutral density.

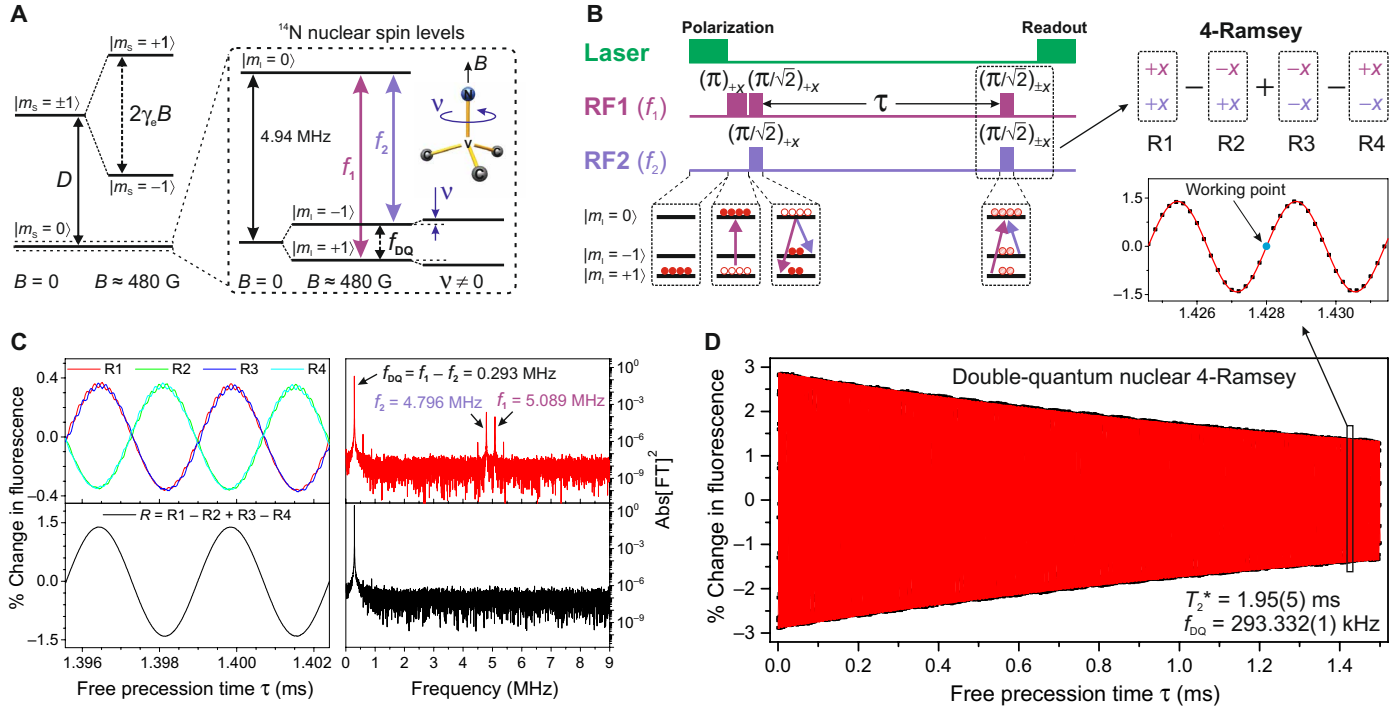

Fig. 2. DQ measurement protocol using ^{14}N nuclear spins in diamond. (**A**) Energy-level diagram of the NV center ground state with and without a magnetic field B applied along the NV axis. The inset depicts the ^{14}N nuclear spin levels, where the splitting between the $|m_I = \pm1\rangle$ sublevels depends on the applied field and on the rotation of the sample around the NV axis. Rotation sensing is based on the measurement of this interval. (**B**) DQ nuclear Ramsey pulse sequence. Inset: 4-Ramsey phase cycling measurement scheme. (**C**) DQ nuclear Ramsey fringes (R1, R2, R3, and R4) obtained by sequentially alternating phases of the last double quantum pulse as depicted in the inset of (B). The frequency-domain spectrum shows the square of the absolute value of the Fourier transform, which reveals DQ signal at f_{DQ} frequency and residual single-quantum (SQ) signals at f_1 and f_2 frequencies. Bottom left: DQ nuclear 4-Ramsey fringes obtained by combining four DQ sequential Ramsey measurements R = R1 − R2 + R3 − R4 to cancel residual SQ signals. (**D**) DQ nuclear 4-Ramsey fringes. Symbols represent experimental data, while the solid line is an exponentially decaying sine wave fit. The oscillation frequency of the signal corresponds to the f_{DQ}, while an exponential decay time corresponds to the nuclear DQ spin coherence time T_2^*= 1.95(5) ms. Inset: Zoomed plot of DQ 4-Ramsey fringes near the working point; rotation measurements were performed at a fixed free precession time $\tau \approx 1.4$ ms by monitoring changes in the fluorescence signal.

$$f_{DQ} = 2B\gamma_n\left(1 - \frac{\gamma_e}{\gamma_n}\frac{A_\perp^2}{D^2 - \gamma_e^2 B^2}\right) \quad (1)$$

where γ_e and γ_n are the electron and nuclear ^{14}N gyromagnetic ratios, respectively; D is the NV electron spin zero-field splitting parameter; and $A_\perp$ is the transverse magnetic hyperfine constant.

The ^{14}N nuclear spins are prepared in a $|m_I = \pm1\rangle$ superposition state and precess about their quantization axis with nuclear precession frequency f_{DQ}. If the diamond rotates about this axis with a frequency ν, then the nuclear precession frequency in the diamond reference frame is $f_{DQ} + 2\nu$ (see Fig. 2A), where the factor of 2 arises from the fact that each state $|m_I = \pm1\rangle$ is shifted by ±ν. The rotation detection presented in this work is achieved by sensitively measuring these frequency shifts using a Ramsey interferometry technique.

Measurement protocol

Figure 2B shows a DQ nuclear Ramsey pulse sequence. A green laser pulse (300-μs duration) initializes the ^{14}N nuclear spins into $|m_I = +1\rangle$ (*25*–*28*). Subsequently, an RF π pulse (frequency f_1; 37-μs duration) is applied to transfer the population into $|m_I = 0\rangle$. Next, to induce a DQ coherence between $|m_I = +1\rangle$ and $|m_I = -1\rangle$, the f_1 and f_2 transitions are simultaneously irradiated with a two-tone $\pi/\sqrt{2}$ resonant RF pulse. Then, after a free precession interval τ, a second two-tone resonant RF pulse is applied to project the phase between the two nuclear spin states $|m_I = \pm1\rangle$ into a measurable population difference, which is read out optically. The DQ nuclear Ramsey sequence leads to population oscillations as a function of τ with a frequency $f_{DQ} + 2\nu$.

RF pulse imperfections, which arise from RF gradients across the sensing volume, lead to the appearance of residual single-quantum (SQ) signals at frequencies f_1 and f_2. These SQ transitions are sensitive to temperature fluctuations, and their signals limit the performance and robustness of the technique. To remove these SQ signals, we implemented a "4-Ramsey" measurement protocol, which was recently demonstrated for the NV electron spins in (*29*); in this work, we extend it to nuclear spins.

The DQ nuclear 4-Ramsey protocol consists of four successive DQ Ramsey sequences with the phase of the second DQ pulse alternated (see Fig. 2B, inset). Figure 2C (top left) demonstrates four optically detected ^{14}N DQ nuclear Ramsey signals (R1 to R4) measured by sequentially alternating the phase of the second DQ pulse at each τ delay. The Fourier transform of the individual DQ Ramsey signals reveal residual SQ signals at f_1 and f_2 frequencies along with DQ signal at f_{DQ} frequency (top right). Residual SQ signals can be eliminated by combining four DQ Ramsey signals in the following way: R = R1 − R2 + R3 − R4 (bottom left). The Fourier transform of the combined DQ 4-Ramsey signal shows no evidence of residual SQ signal (bottom right).

Figure 2D shows the optically detected ^{14}N DQ nuclear 4-Ramsey fringes. Experimental data (symbols) are fit to an exponentially decaying sinusoidal function $R(\tau) = A\, e^{-\tau/T_2^*} \sin(2\pi f_{DQ}\tau + \phi)$ (solid line). From the fit to the Ramsey data, we infer the oscillation frequency f_{DQ} = 293.332(1) kHz and nuclear spin coherence time T_2^* = 1.95(5) ms.

Rotation measurements were performed by implementing the DQ nuclear 4-Ramsey protocol at fixed delay τ_{wp} = 1.428 ms (labeled as working point on Fig. 2D, inset) to detect changes in the phase of the oscillation. The value of τ_{wp} was selected to yield the greatest sensitivity (see section S2). Changes in the DQ 4-Ramsey signal were recorded over time and converted into frequency shifts using a calibration coefficient. This coefficient is determined by the values of τ_{wp} and the amplitude A of the DQ 4-Ramsey fringes in the vicinity of the working point according to the expression $\alpha_0 = 4\pi \cdot \tau_{wp} \cdot A$ and was found to be $\alpha_0 = 6.56(6) \times 10^{-5}$%/(°/s) (see section S3). The dynamic range for the measurement of the rotation rate is discussed in section S4. The bandwidth of the diamond gyroscope is determined by the duration of the DQ 4-Ramsey sequence T_{cycle}, which, under current experimental conditions, is $1/(2T_{cycle}) \approx 70$ Hz.

Diamond gyroscope demonstration and noise characterization

To demonstrate the capabilities of our diamond gyroscope across a range of rotation rates, we performed a series of test experiments on a rate table. First, we performed a calibration of the gyroscope by varying the rotation rate of the platform while measuring the DQ 4-Ramsey fluorescence signal. This was accomplished by repeatedly sweeping the rotation rate between −180 and 180°/s with a linear sweep rate of 1.8°/s^2 and plotting the resulting diamond gyroscope optical output signal against the rate-table rotation rate output, shown in Fig. 3A. The gyroscope output exhibits a linear response over the measured range with a proportionality factor of $\alpha = 6.58(5) \times 10^{-5}$%/(°/s), which agrees with the expected value $\alpha_0 = 6.56(6) \times 10^{-5}$%/(°/s)

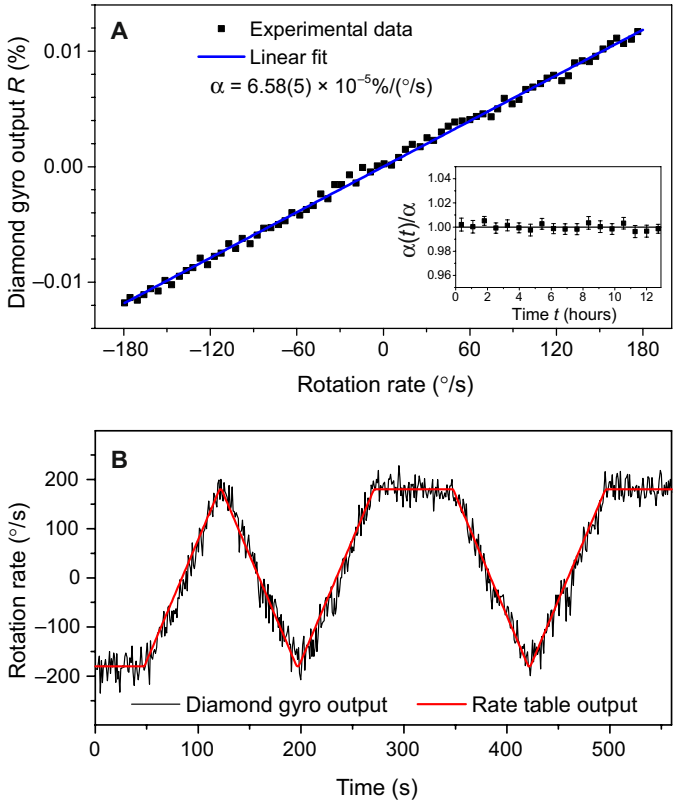

Fig. 3. Diamond gyroscope: Rotation sensing. (**A**) Diamond gyroscope fluorescence signal R measured as a function of the rotation rate of the platform (average of 15 traces; 200 s per trace). The calibration coefficient α is determined from the linear fit. Inset: Time stability of α. Fractional change in α is measured over several hours. (**B**) The rotation rates both measured by the diamond gyroscope and reported by the rate table are averaged over each second and then plotted together as a function of time. The time dependence is programmed to trace "NV."

obtained from analyzing the Ramsey fringes without physically rotating the table.

Next, we used the measured value of α to convert the diamond gyroscope fluorescence signal into a calibrated rotation signal. Figure 3B shows the rate-table output signal (red) and the diamond gyroscope signal (black), which were recorded simultaneously for various rotation sequences.

Figure 4 shows the Allan deviation of the nonrotating diamond gyroscope noise measurement as a function of averaging time. The rotation angle random walk sensitivity of a diamond gyroscope at current experimental conditions is $4.7°/\sqrt{s}$ ($13\ mHz/\sqrt{Hz}$) and is near the photoelectron shot noise limit, which is calculated to be $3.5°/\sqrt{s}$ ($10\ mHz/\sqrt{Hz}$) (see section S3). The uncertainty improves until 300 s and reaches 0.4°/s (1.1 mHz) in bias stability. The dashed dotted line shows a $1/\sqrt{t}$ dependence consistent with frequency white noise.

DISCUSSION

We have demonstrated a solid-state NMR gyroscope based on ^{14}N nuclear spins intrinsic to NV centers in diamond. Key features of the demonstrated technique include the optical polarization and readout of the nuclear spins without the use of microwave transitions and implementation of nuclear DQ Ramsey measurement schemes, which use the entire spin-1 manifold and reduce sensitivity to temperature fluctuations. Through the use of temperature-compensated magnets, magnetic shielding, and robust pulse protocols, we reduce the influence of temperature and magnetic field drift, extending the long-term stability of the gyroscope to hundreds of seconds. The current device demonstrates a sensitivity of $4.7°/\sqrt{s}$ ($13\ mHz/\sqrt{Hz}$) and a bias stability of 0.4°/s (1.1 mHz). These results represent an order of magnitude improvement over those previously achieved with diamond (*18*, *19*). While the current performance of diamond gyroscope is inferior to that of vapor-based NMR gyroscopes, there is still a lot of room for improvement.

The sensitivity can be further improved by at least one order of magnitude by increasing the detected fluorescence, which can be achieved by increasing the laser power and by increasing the photon collection efficiency through improved collection optics and index matching (*30*, *31*). The sensitivity can also be improved by extending the ^{14}N nuclear spin coherence time. The present sensitivity is limited by the ^{14}N nuclear spin T_2^*, which is ~2 ms. However, we have measured the nuclear spin longitudinal relaxation time T_1 to be ~80 s in the same sample. It may be possible to increase the coherence time by up to four orders of magnitude (and improve sensitivity up to two orders of magnitude) using decoupling methods such as spin-bath driving (*32*, *33*).

The long-term stability can be improved by reducing ambient and bias magnetic field drifts. Ambient magnetic field drifts may be reduced with better magnetic shielding, while bias magnetic field drifts can be reduced by temperature stabilization of magnets. Any remaining magnetic field drifts can be corrected using NV electron spin magnetometry (*18*).

In future research, we will use the ^{13}C nuclei ensemble in diamond as an alternative sensing spin species. At the natural abundance, these nuclei provide a higher spin density than ^{14}N intrinsic to NV centers by several orders of magnitude. This in combination with their smaller spin-relaxation rates makes ^{13}C a promising candidate for rotation sensing. However, using the bulk ^{13}C requires development of efficient methods for bulk polarization and spin readout, which is an active area of current research (*34*–*39*).

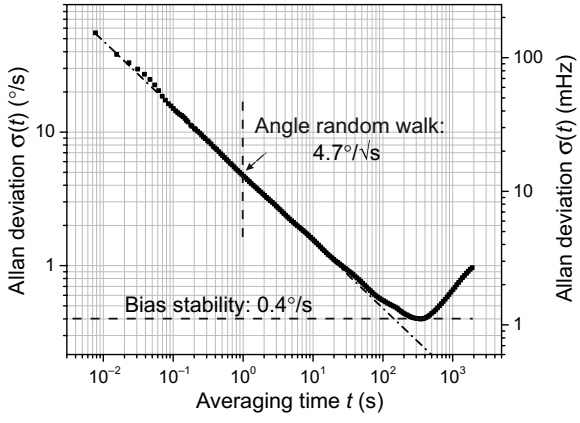

Fig. 4. Diamond gyroscope: Allan deviation. Diamond gyroscope noise measurement as a function of averaging time. The diagonal dash-dotted line shows a $1/\sqrt{t}$ dependence consistent with a white frequency noise.

MATERIALS AND METHODS

The diamond used in our experiments is a ^{12}C-enriched diamond (99.99% ^{12}C) from Element Six. It is a (111)-cut diamond plate (2.5 mm by 1.5 mm by 0.4 mm) grown using chemical vapor deposition with an initial nitrogen concentration of ~13 ppm. NV centers were created by irradiating the sample with 4.5 MeV electrons and subsequent annealing in vacuum at 800°C for 1 hour. The estimated NV concentration is ~4 ppm.

A linearly polarized 515-nm green diode laser light (TOPTICA Photonics iBeam smart 515) was used to excite NV centers in rotation experiments. Laser pulses were generated using an external iBeam smart digital modulation option. In experiments that did not require rotation, we used 532-nm laser (Coherent Verdi G5) due to its superior noise characteristics. Laser pulses for 532-nm laser were generated by passing the continuous-wave laser beam through an acousto-optic modulator. A 0.79–numerical aperture aspheric condenser lens (Thorlabs, ACL25416U-A) was used to illuminate a spot on the diamond with ~80 mW of green light and collect fluorescence. Red fluorescence was separated from the excitation light by a dichroic mirror, passed through a 650- to 800-nm band-pass filter, and detected by a balanced photodetector (Thorlabs, PDB210A), producing ~0.1 mA of photocurrent.

RF pulses with carrier frequencies ($f_1 \approx 5.089$ MHz and $f_2 \approx 4.796$ MHz) were generated by two arbitrary waveform generators (Keysight, 33512B). Each two-channel generator was programmed to output two identical pulses on each channel that are phase shifted by 180° with respect to each other. The pulses with the desired phases were subsequently selected using two transistor-transistor logic (TTL)–controlled RF switches (Mini-Circuits, ZASWA-2-50DR), combined with power combiner (Mini-Circuits, ZFSC-2-6-75), and amplified by an RF amplifier (Mini-Circuits, LZY-22+) (see section S5). RF signals were delivered to the platform via a single-channel RF rotary joint. A TTL pulse card (SpinCore, PBESR-PRO-500) was used to generate and synchronize the pulse sequence. A data acquisition card (National Instruments, USB-6361) was used to digitize experimentally measured signals (see section S4).

SUPPLEMENTARY MATERIALS

Supplementary material for this article is available at https://science.org/doi/10.1126/sciadv.abl3840

REFERENCES AND NOTES

1. V. Passaro, A. Cuccovillo, L. Vaiani, M. De Carlo, C. Edoardo Campanella, Gyroscope technology and applications: A review in the industrial perspective. *Sensors* **17**, 2284 (2017).
2. T. W. Kornack, R. K. Ghosh, M. V. Romalis, Nuclear spin gyroscope based on an atomic comagnetometer. *Phys. Rev. Lett.* **95**, 230801 (2005).
3. E. A. Donley, J. Kitching, Nuclear magnetic resonance gyroscopes, in *Optical Magnetometry*, D. Budker, Derek F. Jackson Kimball, Eds. (Cambridge Univ. Press, 2013), pp. 369–386.
4. T. G. Walker, M. S. Larsen, Chapter eight—Spin-exchange-pumped NMR gyros, in *Advances In Atomic, Molecular, and Optical Physics* (Academic Press, 2016), vol. 65, pp. 373–401.
5. M. E. Limes, D. Sheng, M. V. Romalis, ^{3}He–^{129}Xe comagnetometery using ^{87}Rb detection and decoupling. *Phys. Rev. Lett.* **120**, 033401 (2018).
6. D. A. Thrasher, S. S. Sorensen, J. Weber, M. Bulatowicz, A. Korver, M. Larsen, T. G. Walker, Continuous comagnetometry using transversely polarized Xe isotopes. *Phys. Rev. A* **100**, 061403 (2019).
7. S. S. Sorensen, D. A. Thrasher, T. G. Walker, A synchronous spin-exchange optically pumped NMR-gyroscope. *Appl. Sci.* **10**, 7099 (2020).
8. J. Kitching, Chip-scale atomic devices. *Appl. Phys. Rev.* **5**, 031302 (2018).
9. N. El-Sheimy, A. Youssef, Inertial sensors technologies for navigation applications: State of the art and future trends. *Satellite Navigation* **1**, 2 (2020).
10. M. P. Ledbetter, K. Jensen, R. Fischer, A. Jarmola, D. Budker, Gyroscopes based on nitrogen-vacancy centers in diamond. *Phys. Rev. A* **86**, 052116 (2012).
11. A. Ajoy, P. Cappellaro, Stable three-axis nuclear-spin gyroscope in diamond. *Phys. Rev. A* **86**, 062104 (2012).
12. J. S. Hodges, N. Y. Yao, D. Maclaurin, C. Rastogi, M. D. Lukin, D. Englund, Timekeeping with electron spin states in diamond. *Phys. Rev. A* **87**, 032118 (2013).
13. K. Fang, V. M. Acosta, C. Santori, Z. Huang, K. M. Itoh, H. Watanabe, S. Shikata, R. G. Beausoleil, High-sensitivity magnetometry based on quantum beats in diamond nitrogen-vacancy centers. *Phys. Rev. Lett.* **110**, 130802 (2013).
14. C. L. Degen, F. Reinhard, P. Cappellaro, Quantum sensing. *Rev. Mod. Phys.* **89**, 035002 (2017).
15. K.-M. C. Fu, G. Z. Iwata, A. Wickenbrock, D. Budker, Sensitive magnetometry in challenging environments. *AVS Quant. Sci.* **2**, 044702 (2020).
16. A. Jarmola, I. Fescenko, V. M. Acosta, M. W. Doherty, F. K. Fatemi, T. Ivanov, D. Budker, V. S. Malinovsky, Robust optical readout and characterization of nuclear spin transitions in nitrogen-vacancy ensembles in diamond. *Phys. Rev. Res.* **2**, 023094 (2020).
17. V. V. Soshenko, V. V. Vorobyov, S. V. Bolshedvorskii, O. Rubinas, I. Cojocaru, B. Kudlatsky, A. I. Zeleneev, V. N. Sorokin, A. N. Smolyaninov, A. V. Akimov, Temperature drift rate for nuclear terms of the nv-center ground-state hamiltonian. *Phys. Rev. B* **102**, 125133 (2020).
18. J.-C. Jaskula, K. Saha, A. Ajoy, D. J. Twitchen, M. Markham, P. Cappellaro, Cross-sensor feedback stabilization of an emulated quantum spin gyroscope. *Phys. Rev. Appl.* **11**, 054010 (2019).
19. V. V. Soshenko, S. V. Bolshedvorskii, O. Rubinas, V. N. Sorokin, A. N. Smolyaninov, V. V. Vorobyov, A. V. Akimov, Nuclear spin gyroscope based on the nitrogen vacancy center in diamond. *Phys. Rev. Lett.* **126**, 197702 (2021).
20. V. M. Acosta, E. Bauch, M. P. Ledbetter, A. Waxman, L.-S. Bouchard, D. Budker, Temperature dependence of the nitrogen-vacancy magnetic resonance in diamond. *Phys. Rev. Lett.* **104**, 070801 (2010).
21. H. Kraus, V. A. Soltamov, F. Fuchs, D. Simin, A. Sperlich, P. G. Baranov, G. V. Astakhov, V. Dyakonov, Magnetic field and temperature sensing with atomic-scale spin defects in silicon carbide. *Sci. Rep.* **4**, 5303 (2014).
22. M. Bulatowicz, R. Griffith, M. Larsen, J. Mirijanian, C. B. Fu, E. Smith, W. M. Snow, H. Yan, T. G. Walker, Laboratory search for a long-range *t*-odd, *p*-odd interaction from axionlike particles using dual-species nuclear magnetic resonance with polarized ^{129}Xe and ^{131}Xe gas. *Phys. Rev. Lett.* **111**, 102001 (2013).
23. X. Rong, M. Wang, J. Geng, X. Qin, M. Guo, M. Jiao, Y. Xie, P. Wang, P. Huang, F. Shi, Y.-F. Cai, C. Zou, J. Du, Searching for an exotic spin-dependent interaction with a single electron-spin quantum sensor. *Nat. Commun.* **9**, 739 (2018).
24. J. Ding, J. Wang, X. Zhou, Y. Liu, K. Sun, A. O. Adeyeye, H. Fu, X. Ren, S. Li, P. Luo, Z. Lan, S. Yang, J. Luo, Constraints on the velocity and spin dependent exotic interaction at the micrometer range. *Phys. Rev. Lett.* **124**, 161801 (2020).
25. V. Jacques, P. Neumann, J. Beck, M. Markham, D. Twitchen, J. Meijer, F. Kaiser, G. Balasubramanian, F. Jelezko, J. Wrachtrup, Dynamic polarization of single nuclear spins by optical pumping of nitrogen-vacancy color centers in diamond at room temperature. *Phys. Rev. Lett.* **102**, 057403 (2009).
26. B. Smeltzer, J. McIntyre, L. Childress, Robust control of individual nuclear spins in diamond. *Phys. Rev. A* **80**, 050302 (2009).
27. M. Steiner, P. Neumann, J. Beck, F. Jelezko, J. Wrachtrup, Universal enhancement of the optical readout fidelity of single electron spins at nitrogen-vacancy centers in diamond. *Phys. Rev. B* **81**, 035205 (2010).
28. R. Fischer, A. Jarmola, P. Kehayias, D. Budker, Optical polarization of nuclear ensembles in diamond. *Phys. Rev. B* **87**, 125207 (2013).
29. C. A. Hart, J. M. Schloss, M. J. Turner, P. J. Scheidegger, E. Bauch, R. L. Walsworth, N-V–diamond magnetic microscopy using a double quantum 4-ramsey protocol. *Phys. Rev. Appl.* **15**, 044020 (2021).
30. D. Le Sage, L. M. Pham, N. Bar-Gill, C. Belthangady, M. D. Lukin, A. Yacoby, R. L. Walsworth, Efficient photon detection from color centers in a diamond optical waveguide. *Phys. Rev. B* **85**, 121202 (2012).
31. T. Wolf, P. Neumann, K. Nakamura, H. Sumiya, T. Ohshima, J. Isoya, J. Wrachtrup, Subpicotesla diamond magnetometry. *Phys. Rev. X* **5**, 041001 (2015).
32. G. de Lange, T. van der Sar, M. Blok, Z.-H. Wang, V. Dobrovitski, R. Hanson, Controlling the quantum dynamics of a mesoscopic spin bath in diamond. *Sci. Rep.* **2**, 382 (2012).
33. E. Bauch, C. A. Hart, J. M. Schloss, M. J. Turner, J. F. Barry, P. Kehayias, S. Singh, R. L. Walsworth, Ultralong dephasing times in solid-state spin ensembles via quantum control. *Phys. Rev. X* **8**, 031025 (2018).
34. G. A. Alvarez, C. O. Bretschneider, R. Fischer, P. London, H. Kanda, S. Onoda, J. Isoya, D. Gershoni, L. Frydman, Local and bulk ^{13}C hyperpolarization in nitrogen-vacancy-centred diamonds at variable fields and orientations. *Nat. Commun.* **6**, 8456 (2015).
35. J. P. King, K. Jeong, C. C. Vassiliou, C. S. Shin, R. H. Page, C. E. Avalos, H.-J. Wang, A. Pines, Room-temperature in situ nuclear spin hyperpolarization from optically pumped nitrogen vacancy centres in diamond. *Nat. Commun.* **6**, 8965 (2015).
36. A. Ajoy, K. Liu, R. Nazaryan, X. Lv, P. R. Zangara, B. Safvati, G. Wang, D. Arnold, G. Li, A. Lin, P. Raghavan, E. Druga, S. Dhomkar, D. Pagliero, J. A. Reimer, D. Suter, C. A. Meriles, A. Pines, Orientation-independent room temperature optical ^{13}C hyperpolarization in powdered diamond. *Sci. Adv.* **4**, eaar5492 (2018).
37. D. Pagliero, K. R. K. Rao, P. R. Zangara, S. Dhomkar, H. H. Wong, A. Abril, N. Aslam, A. Parker, J. King, C. E. Avalos, A. Ajoy, J. Wrachtrup, A. Pines, C. A. Meriles, Multispin-assisted optical pumping of bulk ^{13}C nuclear spin polarization in diamond. *Phys. Rev. B* **97**, 024422 (2018).
38. J. Scheuer, I. Schwartz, S. Müller, Q. Chen, I. Dhand, M. B. Plenio, B. Naydenov, F. Jelezko, Robust techniques for polarization and detection of nuclear spin ensembles. *Phys. Rev. B* **96**, 174436 (2017).
39. A. A. Wood, E. Lilette, Y. Y. Fein, V. S. Perunicic, L. C. L. Hollenberg, R. E. Scholten, A. M. Martin, Magnetic pseudo-fields in a rotating electron–nuclear spin system. *Nat. Phys.* **13**, 1070–1073 (2017).

Acknowledgments: We are grateful to P. Kehayias, D. Thrasher, J. Smits, A. Shkel, and A. Wood for helpful discussions. **Funding:** A.J. and S.L. acknowledges support from the U.S. Army Research Laboratory under cooperative agreement nos. W911NF-18-2-0037 and W911NF-21-2-0030. V.M.A. acknowledges support from NSF award no. CHE-1945148, NIH award no. 1DP2GM140921, and a Cottrell Scholars award. This work was supported in part by the EU FET-OPEN Flagship Project ASTERIQS (action 820394) and the German Federal Ministry of Education and Research (BMBF) within the Quantumtechnologien program (grant no. 13N15064). **Author contributions:** The project was conceived by D.B., V.S.M., A.J., and V.M.A. in consultations with A.G.B. and T.I. The experiment was designed by A.J., S.L., and V.M.A. with input from all the authors. P.B. designed and built the magnetic shielding. A.J. constructed the apparatus. S.L. wrote and implemented control and data acquisition software. A.J. and S.L. performed the measurements and analyzed the data with consultation from V.M.A. The project was supervised by V.S.M., T.I., and D.B. All authors discussed the results and contributed to the writing and editing of the manuscript. **Competing interests:** A.J. and D.B. are co-inventors on a related patent application no. US9689679B2. All other authors declare that they have no competing interests. **Data and materials availability:** All data needed to evaluate the conclusions in the paper are present in the paper and/or the Supplementary Materials.

Submitted 9 July 2021
Accepted 1 September 2021
Published 22 October 2021
10.1126/sciadv.abl3840

Citation: A. Jarmola, S. Lourette, V. M. Acosta, A. G. Birdwell, P. Blümler, D. Budker, T. Ivanov, V. S. Malinovsky, Demonstration of diamond nuclear spin gyroscope. *Sci. Adv.* **7**, eabl3840 (2021).